Pis'ma v ZhETF, vol. 94, iss. 2, pp. 146 – 150

Nature of the electronic states involved in the chemical bonding and superconductivity at high pressure in SnO

J. A. McLeod[+1)], *A. V. Lukoyanov*[*,**], *E. Z. Kurmaev*[*], *L. D. Finkelstein*[*], *A. Moewes*[+]

[+]*Department of Physics and Engineering Physics, University of Saskatchewan, 116 Science Place, Saskatoon, Saskatchewan S7N 5E2, Canada*

[*]*Institute of Metal Physics, Russian Academy of Sciences, Ural Division, 620990 Yekaterinburg, Russia*

[**]*Ural Federal University, 620002 Yekaterinburg, Russia*

Submitted 1 June 2011

We have investigated the electronic structure and the Fermi surface of SnO using density functional theory (DFT) calculations within recently proposed exchange-correlation potential (PBE+mBJ) at ambient conditions and high pressures up to 19.3 GPa where superconductivity was observed. It was found that the Sn valence states ($5s$, $5p$, and $5d$ are strongly hybridized with the O $2p$-states, and that our DFT-calculations are in good agreement with O K-edge X-ray spectroscopy measurements for both occupied and empty states. It was demonstrated that the metallic states appearing under pressure in the semiconducting gap stem due to the transformation of the weakly hybridized O $2p$–Sn $5sp$ subband corresponding to the lowest valence state of Sn in SnO. We discuss the nature of the electronic states involved in chemical bonding and formation of the hole and electron pockets with nesting as a possible way to superconductivity.

Guided by research in iron pnictides, superconductivity was observed recently in the layered (α-PbO-type) crystal SnO at high pressure with $T_c = 1.4$ K and $B_{c2} = 0.6$ T at $P = 9.3$ GPa [1]. It was found that electronic structure of SnO at 7 GPa is that of a metal with a hole pocket at the Γ-point and electron pockets at the M-point of Brillouin zone, i.e. both the crystal and electronic structure are similar to those of superconducting iron pnictides (FeAs- and FeSe-based compounds) [1]. On the other hand, unlike the iron pnictides, SnO is nonmagnetic and does not show any structural phase transitions up to $P = 19.3$ GPa [2].

Thus far, the available electronic structure calculations of SnO at high pressure have been performed for high pressures up to 10 GPa (where $V/V_0 = 0.90$) and have been limited to calculation of the $E(k)$ dispersion curves [1, 3–5]. The minor role of Sn $5p$-states near the Fermi level at ambient pressure was examined by Watson [6], he showed that these states are shifted to lower energies due to the hybridized combination of the O $2p$- and Sn $5s$-states just below the Fermi level to provide stability for the litharge structure.

The superconductivity of SnO and layered iron pnictides is increasingly being examined from the perspective of the Fermi surface which is often calculated by density functional theory (DFT). Because the superconductivity of SnO arises during a semiconductor to metal transition, the nature of the band gap closure is important. Since DFT routinely underestimates the magnitude of the band gap [7] it is important to compare the calculated electronic structure to experimental measurements.

In the present paper we have calculated the electronic structure for a range of pressures from ambient to 19.3 GPa using a variety of exchange-correlation functionals, and in particular analyzed the electronic structure and Fermi surface for SnO at $P = 0.0$, 5.1 (the onset of superconductivity [1]), 9.2 (the maximum T_c [1]), and 19.3 (where superconductivity vanishes) GPa.

The calculations on SnO at ambient pressure are compared to non-resonant oxygen K-edge X-ray emission spectroscopy (XES) measurements, performed at Beamline 8.0.1 of the Advanced Light Source (ALS) at Lawrence Berkeley National Laboratory [8], and oxygen K-edge X-ray absorption spectroscopy (XAS) measurements, performed at the spherical grating monochromator beamline of the Canadian Light Source (CLS) at the University of Saskatchewan [9]. The absorption measurements were acquired in the bulk sensitive total fluorescence yield (TFY) mode [10, 11]. Commercially available SnO powder (Alfa Aesar, 99% purity) was used for the spectroscopy measurements. The powder was pressed onto clean indium foil and measured without further preparation.

Our calculations were performed using the WIEN2K code [12] which is based on the full-potential linear augmented plane-wave plus local-orbital (FP-LAPW+lo) method with scalar-relativistic corrections. The spin-

[1)]e-mail: john.mcleod@usask.ca

orbit coupling was not accounted for. For our exchange-correlation functional we have used the local density approximation (LDA) and the Perdew–Burke–Ernzerhof (PBE) variant of the generalized gradient approximation [13]. To improve the calculated band gaps, we have also added a calculation cycle to the PBE-calculation using the modified Becke Johnson (mBJ) exchange potential [14]. We set the cut-off parameter $R_{MT}^{\min}K^{\max}=7$ (the product of the smallest of the atomic sphere radii R_{MT} and the maximum plane-wave wavenumber K) for the expansion of the basis set. The calculation was performed on a $14\times14\times11$ or a $14\times14\times12$ k-point grid for pressures below and above 9 GPa, respectively. The experimental crystal structure of SnO under pressure was used [2]. The same sphere radii were used for both tin and oxygen atoms, and chosen such that the spheres were nearly touching.

The total and partial densities of states (DOS) of SnO at ambient and pressures of 5.1, 9.2, and 19.3 GPa are presented in Fig. 1. At normal conditions

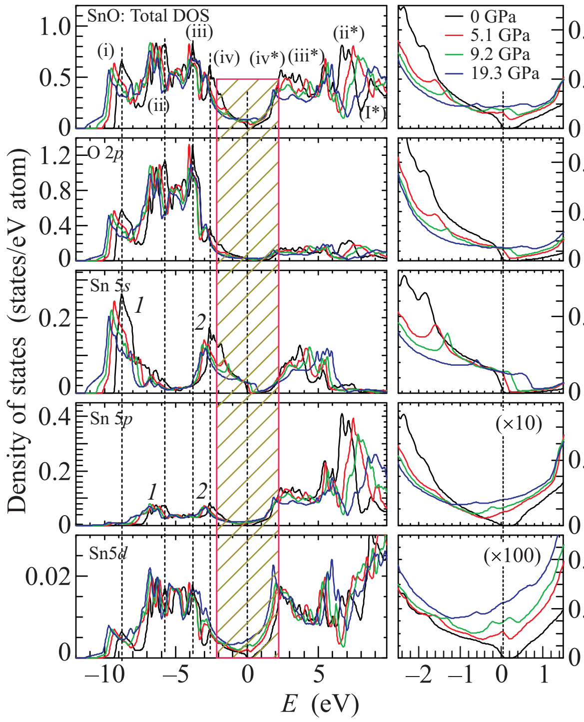

Fig. 1. Total and partial densities of states of SnO for ambient pressure and pressures 5.1, 9.2, and 19.3 GPa. The key bonding (i–iv) and anti-bonding (iv*–i*) features are labeled and discussed in the text. The PBE + mBJ-calculation is shown here, apart from the band gap the other calculations give very similar DOS-spectra

SnO is a semiconductor with a small indirect gap. The LDA-calculation predicts a gap of 0.084 eV, the PBE-calculation predicts a gap of 0.033 eV, and the PBE + mBJ-calculation predicts a gap of 0.254 eV. As one would expect, the O $2p$-states dominate the valence band and mimic the shape of the total DOS. In the conduction band the main contribution near the bottom of the band is again due to O $2p$ hybridized with the Sn $5s$ and $5p$ states. Above 5 eV the Sn $5p$-states are comparable with the O $2p$ states, and the Sn $5s$ contribution becomes almost negligible. McLeod et al. [15] demonstrated that O $2p$-electrons in oxides occupy donor cation states (in our case the Sn $5s$-states) and in addition to this what would normally be considered the nearest excited states (in our case the Sn $5p$ and $5d$ which would formally be considered nonbonding) are involved in chemical bonding.

In the total DOS of SnO, see Fig. 1, one can identify four bonding Sn–O subbands in the occupied part: i, ii, iii, and iv, and corresponding antibonding i*, ii*, iii*, and iv* subbands in the empty part. These bonding and antibonding subbands are almost equally energetically separated from the Fermi level that was used for their identification. The i, ii, and iii subbands are the main bonding subbands of the Sn–O ion-covalent interaction. They have the dominant O $2p$ over the cation contribution and concurrent O $2p$ maximum energy and energies of partial cation maximum, namely, the i subband O $2p$ DOS is located at the Sn $5s(1)$, the ii subband – at the Sn $5p(1)$, the iii subband – at the Sn $5d$. Similar order of states: ns, np, and nd was noted previously in the oxides of the elements of IIb group of the periodic table [15].

The important peculiarity of the partial Sn $5s$- DOS and Sn $5p$-DOS is a separation into two parts 1 and 2, while the main bonding subbands i and ii are formed at the energies of Sn $5s(1)$ and Sn $5p(1)$ separated by approx. 2 eV. In contrast to them, Sn $5s(2)$- and Sn $5p(2)$-parts have the same energy; at this energy the iv weakly bonding subband is formed together with the relatively weak O $2p$ maximum of the DOS. The weak character of the Sn–O bonding in the iv subband is reflected in the comparable contributions of the O $2p$ and Sn $5s$, $5p$, while the O $2p$-states dominate in the i, ii, and iii subbands. In the simplified description of chemical bonding of SnO one would say that this iv subband corresponds to the unbonding electrons responsible for the lowest valence state of Sn, and the i, ii, and iii subbands correspond to the valent-active Sn $5s$, p, d-electrons making strong ion-covalent Sn–O interaction.

Applied pressure results in the approaching interacting Sn and O atoms, and all structural elements in the i–iv subbands are shifted down in energy, demonstrating the increase of bonding effect. The strongest bonding effect can be found for the deepest bonding subbands i and ii. Antibonding subbands iv*–i* under pressure are shifted to the higher energies demonstrating the growth of the antibonding effect.

In the energies from −2 to 2.2 eV the tail parts of the iv and iv* subbands behave differently under pressure. In contrast to the shifts of the main maxima of the iv and iv* subbands, the tail parts are shifted toward each other closing the energy gap and increasing the number of states at the Fermi level, see Figs. 1, 3, 4c. The formation of the metallic states at the Fermi level is shown in detail in the right side of Fig. 1. Thus these metallic states originating from the weakly bonding iv and iv* subbands attribute to the lowest valency state of Sn.

Since the Sn states are involved in hybridization with the O $2p$-states, experimental spectroscopic investigations of the O $2p$-states can reveal significant information about all electronic states of SnO. The calculated O $2p$ DOS for SnO at ambient pressure is compared with measured XES (probing the valence states) and XAS (probing the conduction states) spectra in Fig. 2. The O K-edge XES reproduces the calculated O $2p$ valence states accurately, and decomposing the measured spectrum into 4 pseudo-Voigt components reproduces three of the four valence intervals. The last interval (iv) is likely hidden in the experimentally broadened edge of the much larger iii interval. The O K-edge XAS-spectrum are also found in good agreement with the calculated spectrum.

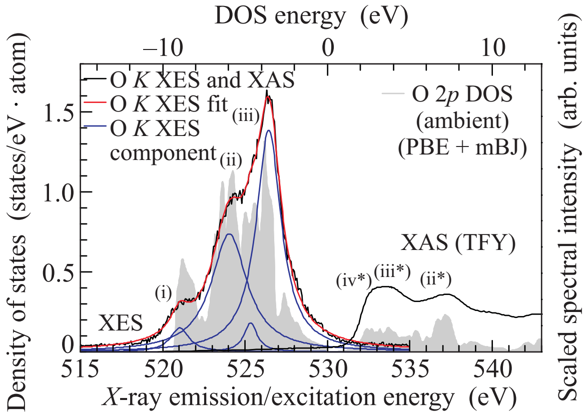

Fig. 2. The measured O K-edge XES and XAS. The XES-spectrum has been fit with 4 pseudo-Voigt components, three of which agree with the previously discussed valence band intervals. The ambient O $2p$ DOS is also plotted, it has been aligned with the XES-spectrum. The XAS-spectrum shows the same two intervals as the calculated DOS

At ambient pressure we find the top of the valence band is formed by a dispersive band approaching the Γ-point, in agreement with the previously reported calculations [1, 3]. This band corresponds to the Sn $5s$-states hybridized with the O $2p$-states, as shown in the partial DOSes in Fig. 1 and the Sn $5s$ contribution to the bands in Fig. 3. Increasing pressure results in the broadening of this band and causes the appearance of a hole pocket near the Γ-point. Increasing pressure also causes the appearance of electron pockets near the M-point due to the broadening of bands having a little Sn $5s$ contribution in comparison with the subband in the Γ-point. The calculations for all exchange-correlation functionals predict the same general shape of the electron pocket at the Fermi level for SnO under high pressure, while the different exchange-correlation functionals predict slightly different sizes for the hole pocket. The direct gap at the Γ-point is 2.1 eV for the LDA- and PBE-calculations, and 2.5 eV for the PBE + mBJ-calculation. Early measurements of the optical gap in polycrystalline SnO suggest the gap should be between 2.5 and 3.0 eV [16].

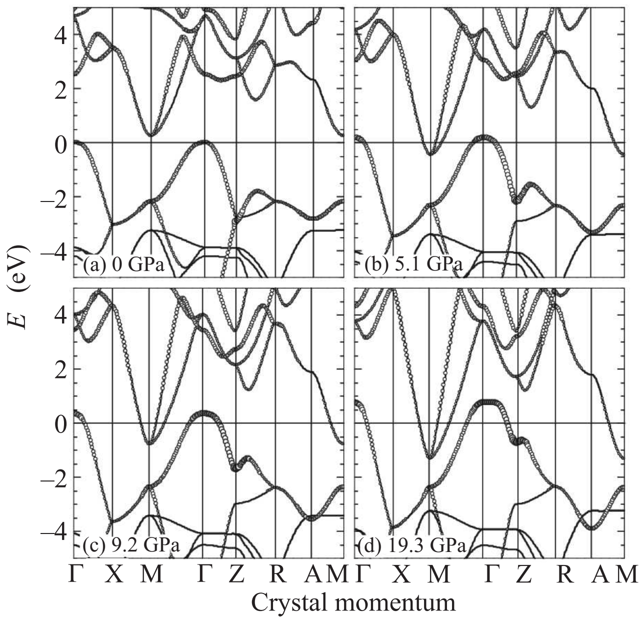

Fig. 3. Band structure plots of SnO at ambient, 5.1, 9.2, and 19.3 GPa calculated with the PBE + mBJ exchange-correlation functional. The Sn $5s$ contribution to the band structure is proportional to the width of the line

The correlation between the valence O $2p$-states and the Sn $5s$, $5p$, $5d$-states tells a more nuanced story. The correlation here is defined as $C_a(E) = \int \rho_{O2p}(E')\rho_a(E-E')dE'$ for partial DOS ρ_i, where a = Sn $5s$, $5p$, or $5d$. This function determines the degree of similarity between two spectra, and the energy of the peak of this function indicates the overall shift between the two spectra. This energy shift is shown in Fig. 4b. Note that while the Sn $5s$-states contribute to the hole pocket at

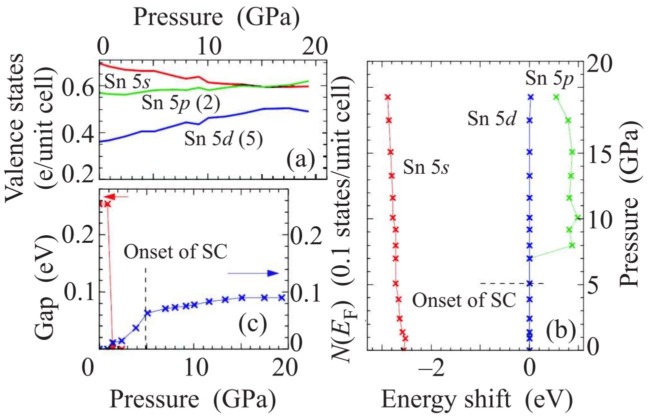

Fig. 4. The number of valence states of Sn (**a**), the correlation shift between the Sn and O 2p-states (**b**), and the band gap and number of states at the Fermi level (**c**)

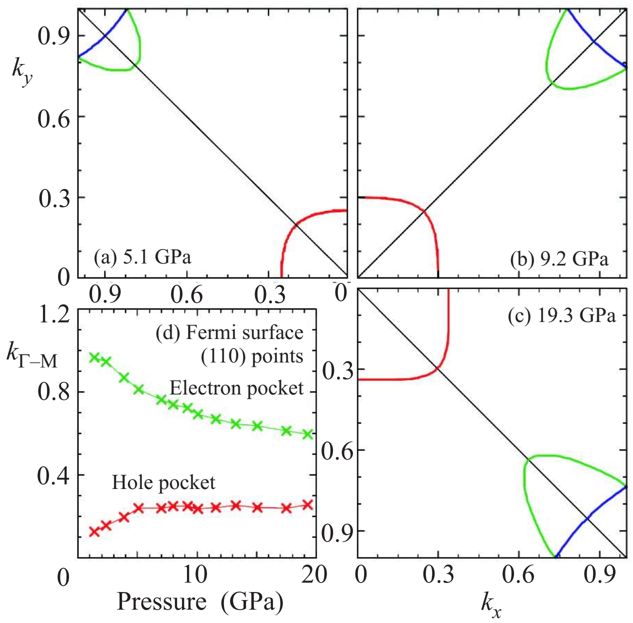

Fig. 5. One quadrant of the Fermi surface in the k_x, k_y plane (at $k_z = 0$) for SnO at 5.1 (**a**), 9.2 (**b**), and 19.3 GPa (**c**), calculated with the PBE + mBJ functional. Since our calculation suggests SnO at ambient pressures is an insulator, the Fermi surface in this case is trivial. In panel **d**, the nesting vector in the (110) direction from the corner of the Γ-point hole band to the opposite outer M- point electron band is also shown for various pressures

the Fermi level, the bulk of the Sn 5s-states are at lower energies than the O 2p-states. Further, as pressure increases, the Sn 5s-states shift to lower energies faster than the O 2p states. The 5d-states, which contribute minimally to the valence band, almost exactly track the position of the O 2p-states in energy. Most importantly is that PBE + mBJ calculation predicts that the Sn 5p-states shift to higher energies than the O 2p- states roughly concurrent with the onset of superconductivity (at 7 GPa, rather than 5.1 GPa). This is related to the increased influence of the electron pockets at the M-point.

Another change in the electronic structure concurrent with the onset of superconductivity is the saturation of the number of states at the Fermi level ($N(E_\mathrm{F})$), shown in Fig. 4c. While the number of states at the Fermi level increases immediately after applied pressure has closed the band gap, $N(E_\mathrm{F})$ starts to saturate at 5.1 GPa in Fig. 4c. This is because the low pressure grown in $N(E_\mathrm{F})$ is mainly driven by increasing contributions of O 2p- and Sn 5s-states which reach a maximum at 5.1 GPa, while the Sn 5p-states continue to increase their contribution this is only a minor addition to the total number of states (see the right side Fig. 1).

As seen from the experiment and the calculated partial DOSes in Fig. 1, the states near the Fermi level mostly contain O 2p-states, hybridized with the Sn 5s and 5p-states. With increasing pressure these states are distorted into an increasing hole pocket at the Γ-point and two increasing electron pockets at the M-point, see Fig. 5. The distance between these two surfaces in the (110) direction decreases with increasing pressure, and the electron pockets grow faster than the hole pocket. In particular note that in Fig. 3 the behaviour of the bands at the Fermi surface is essentially identical in the Γ–X-direction. As one can see from Fig. 6 showing the number of states at the Fermi level from electron and hole pockets, the hole carriers dominate over the whole region of superconductivity in SnO. The difference of the (hole band)–(inner and outer electron bands) carriers tracks the behaviour of T_c suggesting the hole-type of superconductivity in SnO at high pressure.

In conclusion, we have investigated electronic structure and Fermi surface of SnO at ambient and high pressures to clarify the electronic states near the Fermi level involved in chemical bonding and superconductivity using *ab initio* calculations. It was found that the semiconducting gap in SnO is closed under pressure by the weakly hybridized O 2p- Sn 5s-, p-states, located in the semiconductor SnO near the top of the valence band and the bottom of the conduction band. These states stabilize the lowest valence state of Sn but don't take part in strong ion-covalent O 2p–Sn 5s, p, d interaction in the Sn–O layers. Under pressure they become more metallic and their tail parts fill the energy gap due to the increase of Sn–Sn interaction of the nearest layers. It seems that compounds with cations in the lowest valency are perspective for new superconductors, and the marked similarity of SnO with FeSe and Fe-pnictide based su-

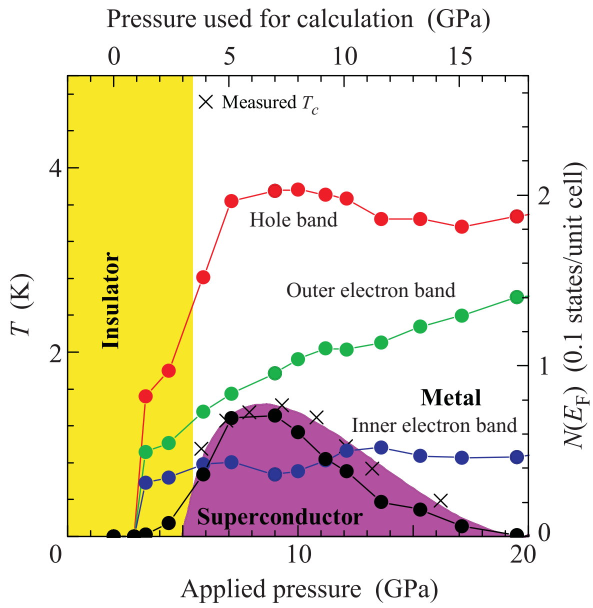

Fig. 6. Number of states at the Fermi level of the bands forming electron and hole pockets and their difference (hole band)–(inner and outer electron bands) vs. pressure. For comparison the phase diagram and pressure dependence of superconducting transition temperature from [1] are given accounting for the underestimated by 1.5 GPa energy gap closure in the calculation

perconductors is probably not accidental. With the increasing pressure the size of hole and electron pockets at the Γ- and M-points, respectively, increases, leading to the nesting effect possibly involved in the formation of superconductivity.

We acknowledge support of the Russian Foundation for Basic Research (Projects # 11-02-00022, 10-02-00046, and 10-02-00546), the Natural Sciences and Engineering Research Council of Canada (NSERC), the Canada Research Chair program, # MK-3376.2011.2, the scientific program of the Russian Federal Agency of Science and Innovation under Project # 02.740.11.0217, partial support of the scientific program "Development of Scientific potential of Universities" under Project # 2.1.1/779 and the scientific program of the Russian Federal Agency of Science and Innovation under Project # 02.740.11.0217.

1. M. K. Forthaus, K. Sengupta, O. Heyer et al., Phys. Rev. Lett. **105**, 157001 (2010).
2. X. Wang, F. X. Zhang, I. Loa et al., Phys. Status Solidi B **241**, 3168 (2004).
3. N. E. Christensen, A. Svane, and E. L. Peltzer y Blancá, Phys. Rev. B **72**, 014109 (2005).
4. N. E. Christensen, I. Gorczyc, and A. Svane, J. Phys. Chem. Sol. **67**, 1948 (2006).
5. I. Lefebvre, M. A. Szymanski, J. Olivier-Fourcade, and J. C. Jumas, Phys. Rev. B **58**, 1896 (1998).
6. G. W. Watson, J. Chem. Phys. **114**, 758 (2001).
7. P. Dufek, P. Blaha, and K. Schwarz, Phys. Rev. B **50**, 7279 (1994).
8. J. J. Jia, T. A. Callcott, J. Yurkas et al., Rev. Sci. Instrum. **66**, 1394 (1995).
9. T. Regier, J. Krochak, T. K. Sham et al., Nucl. Instrum. Methods Phys. Res. A **582**, 93 (2007).
10. D. W. Boukhvalov, E. Z. Kurmaev, A. Moewes et al., Phys. Rev. B. **67**, 134408 (2003).
11. S. J. Kang, Y. Yi, C. Y. Kim et al., Appl. Phys. Lett. **86**, 232103 (2005).
12. P. Blaha, K. Schwarz, G. K. H. Madsen et al., **WIEN2k**, An Augmented Plane Wave + Local Orbitals Program for Calculating Crystal Properties, (Karlheinz Schwarz, 2001), Techn. Universität Wien, Austria, ISBN 3-9501031-1-2.
13. J. P. Perdew, K. Burke, and M. Ernzerhof, Phys. Rev. Lett. **77**, 3865 (1996).
14. F. Tran and P. Blaha, Phys. Rev. Lett. **102**, 226401 (2009).
15. J. A. McLeod, R. G. Wilks, N. A. Skorikov, Phys. Rev. B **81**, 245123 (2010).
16. J. Guerts, S. Rau, W. Ritcher, and F. J. Schmitte, Thin Solid Films **121**, 217 (1984).